

# Backbone and side chain assignment strategies for multiply labeled membrane peptides and proteins in the solid state

Aneta T. Petkova,<sup>a,b,1</sup> Marc Baldus,<sup>b,2</sup> Marina Belenky,<sup>a</sup> Mei Hong,<sup>b,3</sup>  
Robert G. Griffin,<sup>b,\*</sup> and Judith Herzfeld<sup>a</sup>

<sup>a</sup> Department of Chemistry and Keck Institute for Cellular Visualization, Brandeis University, Waltham, MA 02454-9110, USA

<sup>b</sup> Department of Chemistry and Francis Bitter Magnet Laboratory, Massachusetts Institute of Technology, Cambridge, MA 02139, USA

Received 18 October 2001; revised 30 September 2002

## Abstract

We demonstrate that the SPECIFIC CP technique can be used to obtain heteronuclear correlation (HETCOR) spectra of peptide backbones with greater efficiency than conventional HETCOR methods. We show that similar design principles can be employed to achieve selective homonuclear polarization transfer mediated through dipolar or scalar couplings. Both approaches are demonstrated in a tripeptide with uniform <sup>15</sup>N and <sup>13</sup>C labeling, and with uniform <sup>15</sup>N labeling and natural abundance <sup>13</sup>C. In other applications, the high efficiency of the heteronuclear SPECIFIC CP transfer allows discrimination of single amide signals in the 248-residue membrane protein bacteriorhodopsin (bR). In particular, variations are detected in the ordering of the Ala81–Arg82 peptide bond among the photocycle intermediates of bR and SPECIFIC CP is used to correlate <sup>15</sup>N and <sup>13</sup>C signals from the three Val–Pro peptide bonds.

© 2002 Elsevier Science (USA). All rights reserved.

**Keywords:** Bacteriorhodopsin; Cross polarization; Heteronuclear and homonuclear correlations; Magic angle spinning; Solid state NMR

## 1. Introduction

Much of the success of nuclear magnetic resonance (NMR)<sup>4</sup> for the study of soluble biomolecules relies on

\* Corresponding author. Fax: 617-253-5405.

E-mail addresses: [griffin@ccnmr.mit.edu](mailto:griffin@ccnmr.mit.edu), [rgg@mit.edu](mailto:rgg@mit.edu) (R.G. Griffin).

<sup>1</sup> Present address: Laboratory of Chemical Physics, NIDDK, National Institutes of Health, Bethesda, MD 20892, USA.

<sup>2</sup> Present address: Max-Planck-Institute for Biophysical Chemistry, Am Fassberg 11, 37077 Göttingen, Germany.

<sup>3</sup> Present address: Department of Chemistry, Iowa State University, Ames, IA 50011, USA.

<sup>4</sup> Abbreviations used: bR, bacteriorhodopsin; CP, cross polarization; CW, continuous wave; DA, dark-adapted resting state of bR; LA, light-adapted resting state of bR in which the Schiff base (SB) is protonated and Asp-85 is deprotonated; *M<sub>o</sub>*, a bR photocycle intermediate in which the SB is deprotonated and Asp-85 is protonated; MAS, magic angle spinning; f-MLF-OH, *N*-formyl-L-methionyl-L-leucyl-L-phenylalanine-OH; NMR, nuclear magnetic resonance; SPECIFIC CP, spectrally induced filtering in combination with CP; SSNMR, solid-state NMR; S/N, signal-to-noise; DQ, double quantum; SQ, single quantum; ZQ, zero quantum.

heteronuclear and homonuclear correlation techniques to establish multiple intra- and inter-residue connectivities [1]. Analogous experiments for the study of immobilized systems, i.e., membrane and amyloid proteins, are highly desirable. An important constraint is that such experiments not degrade the resolution or signal-to-noise (S/N) of the spectrum. This consideration applies regardless of whether the spectrum is acquired from a sample spinning at the magic angle (MAS) [2,3] or from an aligned sample [4–6].

Recently we proposed an approach that satisfies these requirements in the context of heteronuclear polarization transfer without restricting the number or the position of the isotopic labels, i.e., <sup>13</sup>C and <sup>15</sup>N [7]. This technique, SPECIFIC CP, is based on the conventional cross polarization method [8,9] originally developed to enhance the polarization and shorten the spin–lattice relaxation times of low- $\gamma$  nuclei such as <sup>13</sup>C or <sup>15</sup>N via contact with abundant protons. Under normal circumstances, a broadband and efficient transfer to the low- $\gamma$  nucleus is established by using r.f. fields that significantly exceed the

spectral range. More recently these were combined with ramped or adiabatic amplitude modulations [10–12]. Such approaches are equally applicable to broadband heteronuclear correlation experiments [13].

In studies of polypeptides and proteins in liquid state it is usually sufficient to examine a succession of two-spin correlations such as in NH-CA, NH-CA-CB or NH-CA-CO topologies. In a conventional HETCOR experiment [14] this is usually achieved by a decrease of the spectral sampling window. Obviously, a technique that would selectively correlate particular chemical shift regions of the spectrum would have the advantage of increased transfer efficiencies due to a smaller number of coupling partners in addition to simplified structural analysis. Fig. 1 illustrates the transfer characteristics for conventional CP with decreasing r.f. fields. It is apparent that the CP method can be tailored for band selectivity (uniform high transfer efficiency over a range of several kHz), e.g.,  $-5$  to  $5$  kHz in Fig. 1b, or frequency specific transfers (high transfer efficiency over a range of only several Hz), e.g., at  $|12|$  kHz in Fig. 1c and at  $|9|$  kHz in Fig. 1d if carefully chosen r.f. fields ( $\omega_{11}$  or  $\omega_{1S}$ ) and frequency offsets ( $\Omega_1$  or  $\Omega_S$ ) are used. In general, hetero- and homo-nuclear (i.e.,  $\omega_{11} = \omega_{1S}$ ) two-spin polarization transfer is established, if the applied CW r.f. irradiation and MAS frequency fulfill the following condition:

$$\sqrt{\Omega_1^2 + \omega_{11}^2} \pm \sqrt{\Omega_S^2 + \omega_{1S}^2} = n\omega_R, \quad (1)$$

where  $\omega_R$  is the MAS frequency, and  $\Omega_{1(S)}$  and  $\omega_{11(S)}$  are the chemical shift offset and r.f. field of the I (S) spin. It can be shown that the positive sign in Eq. (1) leads to double-quantum (DQ) polarization transfer for both heteronuclear [7,15] and homonuclear [16] spin systems. Zero-quantum (ZQ) transfer results if the difference of the effective fields (the negative sign in Eq. (1)) matches a multiple of the MAS frequency. For each value of  $n$ , it is possible to calculate the effective transfer rate given by the coupling. For  $n = 0$ , Eq. (1) describes the transfer characteristics for an isotropic scalar coupling (i.e., isotropic oscillatory transfer) if  $|\Omega_1| = |\Omega_S|$  [13]. Note that to lowest order average Hamiltonian theory, this condition is independent of the size of the applied r.f. field. Dipolar couplings are recovered during MAS under the conditions  $n = 1$  and  $n = 2$ . Higher orders of  $n$  may result from chemical shielding interactions or multi-spin interactions.

As shown in Fig. 1 for a heteronuclear spin pair, the transfer characteristics depend on the size and the relative ratio of applied r.f. fields and MAS frequency. Note that the curves obtained in Fig. 1 are equally valid for a homo- and a heteronuclear spin pair. Note also that ZQ/DQ conditions are generally given by a positive and negative transfer maximum, respectively [17]. In general, the  $n = 1$  recoupling condition, with

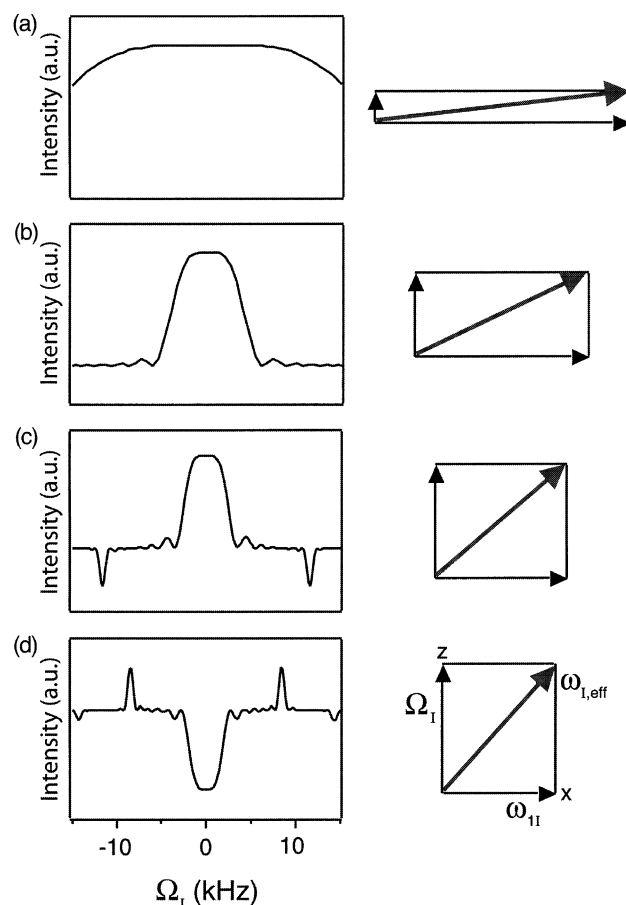


Fig. 1. Simulations of on-resonance ( $\Omega_S = 0$ ) polarization transfer as a function of the r.f. fields and offsets in a heteronuclear two-spin system. The normalized transfer efficiency vs. the offset for the non-observe I spin is displayed on the left. A schematic representation of the relative amplitude of the r.f. field and the offset of the I spin in each case is shown on the right. The simulations were conducted within the GAMMA simulation environment [44] employing a piecewise constant approximation of the MAS induced time dependence of the system Hamiltonian. Signal intensities were obtained by co-adding transfer amplitudes of  $> 2 \times 10^4$  randomly oriented single crystal orientations and assuming a one-bond N–C dipolar coupling of 900 Hz. The following r.f. field strengths were used: (a)  $\omega_{11}/2\pi = 500$  kHz,  $\omega_{1S}/2\pi = 509$  kHz; (b)  $\omega_{11}/2\pi = 20$  kHz,  $\omega_{1S}/2\pi = 29$  kHz; (c)  $\omega_{11}/2\pi = 2$  kHz,  $\omega_{1S}/2\pi = 11$  kHz; and (d)  $\omega_{11}/2\pi = 2$  kHz,  $\omega_{1S}/2\pi = 7$  kHz. In all cases  $\omega_R/2\pi = 9.0$  kHz and  $t_{SP} = 5.0$  ms. For simplicity, the scalar coupling was neglected. Note that the degree of selectivity is directly related to the relative size of r.f. field strength and carrier offset. In (a) the matching condition is largely unaffected by variations in the carrier frequency ( $\Omega_1 \ll \omega_{11}$ ) while in (d) both parameters are of comparable size ( $\Omega_1 \approx \omega_{11}$ ).

its stronger dipolar coupling, is preferred for highly efficient transfer. Furthermore the DQ condition ( $n = 1$ , positive sign in Eq. (1)) is preferable for small r.f. fields and moderate MAS frequencies, and can be used when relatively high efficiency and only band selectivity is desired (Fig. 1d).

In this contribution, we present applications of the heteronuclear SPECIFIC CP technique in a tripeptide

and discuss design principles for directing polarization transfer among homonuclear spins in a highly selective manner. Both methods can be employed using small or moderate r.f. fields and allow for unequivocal data interpretation. Using *N*-formyl-[U-<sup>13</sup>C, <sup>15</sup>N] methionyl-leucyl-phenylalanine-OH, we demonstrate, with a series of 1D dipolar transfer experiments, that these methods can be used to map out the complete backbone and side chain correlation pattern. SPECIFIC CP recoupling is characterized by simple algebraic transfer, and therefore the results can be employed to reconstruct the NH-C<sub>α</sub> intra-residue connectivity pattern without the need of a two-dimensional HETCOR experiment. We also demonstrate the high transfer efficiency of SPECIFIC CP using a <sup>15</sup>N-labeled sample of the peptide with natural abundance <sup>13</sup>C.

The excellent efficiency of the technique makes it practical for backbone studies in a 26-kDa integral membrane protein, bacteriorhodopsin (bR). bR functions as a light-driven proton pump in the plasma membranes of *Halobacterium salinarum*. The chain of 248 amino acid residues is organized into seven trans-membrane helices [18,19]. The chromophore is a retinal Schiff base (SB) formed with Lys216. Upon illumination, the chromophore isomerizes, the Schiff base deprotonates and reprotonates, and the retinal re-isomerizes. These events are accompanied by other changes that result in proton release and uptake on opposite sides of the membrane. The net effect is transport of a single proton from the cytoplasm to the extracellular medium in the course of the photocycle. The resulting electrochemical potential gradient is used by the cell for its energetic requirements.

In the resting state of bR, the side chain of Arg82 is thought to participate in the hydrogen-bonded complex counterion of the SB. As one of the few ionizable amino acid residues in the proton pathway, its role in the proton-motive photocycle of bR has been studied extensively by site-specific mutagenesis [20–24]. In addition, recent solid-state NMR experiments [25] have detected significant changes in an arginine side chain during the bR photocycle which have been tentatively assigned to Arg82. Investigations of the amide signals of the seven arginine residues in bR indicate that more than one of the resonances changes during the photocycle, and it is conceivable that Arg82 might be involved in some of the perturbations. To isolate and monitor structural changes in the Ala81–Arg82 peptide bond, we used SPECIFIC CP to investigate [1-<sup>13</sup>C]Ala, [U-<sup>15</sup>N]Arg, [ζ-<sup>15</sup>N]Lys-bR. Significant chemical shift and lineshape changes in the spectra suggest varying degrees of disorder in the Ala81–Arg82 peptide bond during the bR photocycle.

We also utilize the SPECIFIC CP technique to correlate the carbonyl and amide signals from the three Val–Pro peptide bonds in [α-<sup>15</sup>N]Pro, [1-<sup>13</sup>C]Val-bR.

The Val49–Pro50 pair is situated in helix B, and, like other proline residues embedded in integral membrane proteins, is considered to have the potential to facilitate functionally important conformational changes. The other two pairs, Val69–Pro70 and Val199–Pro200, are located at the extracellular surface of the protein, in the BC and FG loop, respectively. The results indicate the potential of SPECIFIC CP for backbone studies in systems with heavy spectral overlap and low signal-to-noise.

## 2. Materials and methods

### 2.1. Samples

*N*-Formyl-MLF-OH, whose molecular structure is shown in Fig. 2, was prepared using solid phase synthesis methods by American Peptide Corporation (Sunnyvale, CA) using Fmoc chemistry and <sup>15</sup>N (Met: 95–99%, Leu and Phe: 98%+) or <sup>13</sup>C, <sup>15</sup>N (Met, Leu, and Phe: <sup>13</sup>C, 98%+, <sup>15</sup>N, 96–99%) labeled amino acids obtained from Cambridge Isotope Laboratories (Andover, MA). Note that the amino acid residues were isotopically labeled, but the formyl group was not. Precipitation of the solid sample of f-MLF-OH was from 2-propanol and is described elsewhere [26].

[1-<sup>13</sup>C]Ala, [U-<sup>15</sup>N]Arg, [ζ-<sup>15</sup>N]Lys-bR was prepared by growing an arginine auxotrophic strain of *H. salinarum* [25] in a medium similar to that of [27] except that L-[1-<sup>13</sup>C]Ala, L-[U-<sup>15</sup>N]Arg, and L-[ζ-<sup>15</sup>N]Lys replaced their unlabeled counterparts. The incorporation of the labeled amino acids was traced with L-[1-<sup>14</sup>C]Ala, L-[ζ-<sup>14</sup>C]Arg, and L-[4,5-<sup>3</sup>H<sub>2</sub>]Lys in parallel preparations. No scrambling of the radioactive label to other residues in the protein was detected, although ~45% of the radioactivity incorporated from L-[1-<sup>14</sup>C]Ala and ~45% of the radioactivity incorporated from L-[4,5-<sup>3</sup>H<sub>2</sub>]Lys was extracted with the lipids and the chromophore. The labeling of the alanine, arginine, and lysine residues was 76%, 88%, and 58%, respectively.

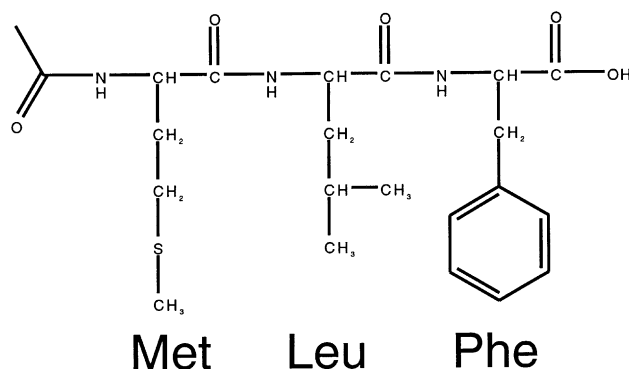


Fig. 2. The molecular structure of *N*-formyl-MLF-OH.

[ $\alpha$ - $^{15}\text{N}$ ]Pro, [ $1$ - $^{13}\text{C}$ ]Val-bR was prepared by growing the JW-3 strain of *H. salinarum* in a medium with unlabeled proline and valine replaced by L-[ $\alpha$ - $^{15}\text{N}$ ]proline and L-[ $1$ - $^{13}\text{C}$ ]valine, respectively. Trace L-[U- $^{14}\text{C}$ ]proline and L-[U- $^{14}\text{C}$ ]valine were introduced in the medium in order to estimate the incorporation rates. Only 4–5% of the radioactivity incorporated from proline and valine was extracted with the lipids and the chromophore, and previous data [28,29] showed no scrambling of the label from proline and valine to other amino acid residues. The labeling of both the proline and valine residues were 100%.

The bR containing purple membrane patches were isolated in the usual manner [30]. An appropriately conditioned purple membrane pellet was obtained following the procedure outlined in [25] and packed in a transparent 5-mm pyrex rotor (Wilmad Glass, Buena, NJ). Light was delivered to the sample via a glass optic fiber bundle with the end positioned at the middle of the 5-mm spinner module. The light-adapted (LA) state of bR was obtained after several hours of illumination of dark-adapted (DA) bR at 0–1 °C, with white light from a 1000-W Xe lamp (Oriol Instruments, Stratford, CT), directed through a water filter and an IR blocking filter (Oriol Instruments) to reduce heating. The  $M_0$  photointermediate was accumulated by illumination of LA bR in 0.3 M guanidyl chloride, pH = 10 with  $\lambda > 550$  nm (long pass filter from Oriol Instruments) for one hour at about –60 °C. The photocycle intermediates were preserved in the dark between –90 and –100 °C for the duration of data acquisition. For the experiments with [ $\alpha$ - $^{15}\text{N}$ ]Pro, [ $1$ - $^{13}\text{C}$ ]Val-bR, the dark-adapted state of the protein was studied at 0–1 °C to benefit from the improved overall resolution at this elevated temperature.

## 2.2. Solid-state NMR

The SSNMR experiments were performed on custom-built spectrometers operating at  $^1\text{H}$  frequencies of 500.1, 397.8, and 317.6 MHz. Quadruple and triple resonance transmission line probes [31] equipped with 4-mm Chemagnetics spinner modules (Fort Collins, CO) were used in the *N*-formyl-MLF-OH studies, and a quadruple resonance transmission line probe equipped with a 5-mm Chemagnetics spinner module and a stainless steel dewar for lower temperatures was used for the bR experiments. The MAS spectra were obtained by either constant or ramped amplitude Hartmann–Hahn cross polarization (CP) [8,9] or by SPECIFIC CP [7], both with TPPM decoupling during data acquisition [32], as illustrated in the pulse sequence of Fig. 3. Typical r.f. fields were 100 kHz for  $^1\text{H}$  decoupling; 40 kHz (CP) and 1–20 kHz (SPECIFIC CP) for  $^{13}\text{C}$ ; and 35 kHz (CP) and 5–20 kHz (SPECIFIC CP) for  $^{15}\text{N}$ . The low amplitude r.f. fields were measured in [ $1,2$ - $^{13}\text{C}_2$ ]acetyl-[1-

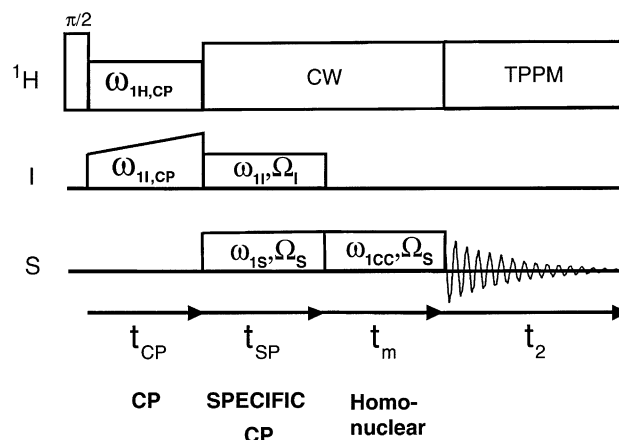


Fig. 3. Experimental scheme to establish combined heteronuclear and homonuclear polarization transfer under MAS. An initial broadband cross polarization from protons to nitrogen is followed by a SPECIFIC CP [7] transfer step to create CO or  $C_\alpha$  polarization, and then, if desired, by a homonuclear polarization transfer with variable r.f. field strength and mixing time  $t_m$ . TPPM decoupling [32] is applied during  $^{13}\text{C}$  signal acquisition. Alternatively, the same sequence is used if the  $^{15}\text{N}$  spins need to be observed. Further details are given in the text and in the figure legends for the actual experiments.

$^{15}\text{N}$ ]valine. Initial values were estimated from on-resonance nutation experiments. Subsequently, SPECIFIC CP transfer curves (stepping of the frequency offset on the non-observe channel, usually for two sets of r.f. fields) were obtained and compared to simulations. Very small or no adjustments of the r.f. amplitudes had to be made in order to fit the experimental data. Homonuclear polarization transfer was established using CW irradiation of variable amplitude  $\omega_{1CC}$  on the  $^{13}\text{C}$  channel. The usual TPPM pulse angle was 170°, and the phase was 45° or 15°. Spectra were collected with 2 ms CP contact time, 1.5–2.5 ms SPECIFIC CP contact time, and 1–5 ms mixing times ( $t_m$ ) in experiments involving side chain resonances. Data points (1024) were acquired using a dwell time of 20  $\mu\text{s}$ . The recycle delay was 3 s for f-MLF-OH, and 2 or 3 s for bR. The  $^{13}\text{C}$  chemical shifts are referenced to TMS with adamantane as a secondary standard (peaks at 38.56 and 29.50 ppm [33]). The  $^{15}\text{N}$  chemical shifts are referenced to liquid  $\text{NH}_3$  by using the  $^{15}\text{N}/^{13}\text{C}$  frequency ratios [34], and the chemical shift of TMS relative to DSS (+1.7 ppm [35]). All shifts bear a 0.4 ppm uncertainty.

Our previous work [7] discusses in detail the dependence of the SPECIFIC CP transfer efficiency on the r.f. field amplitudes and frequency offsets (see Eq. (19) and Fig. 4 in [7]). In the present work, we elaborate the SPECIFIC CP experiment by retaining the carrier offset on the non-observe channel as a variable, rather than adjusting the fields to the isotropic chemical shift values. It therefore follows from Eq. (1) that recoupling of a heteronuclear spin pair ( $r$ ) occurs whenever the resonance offset fulfills

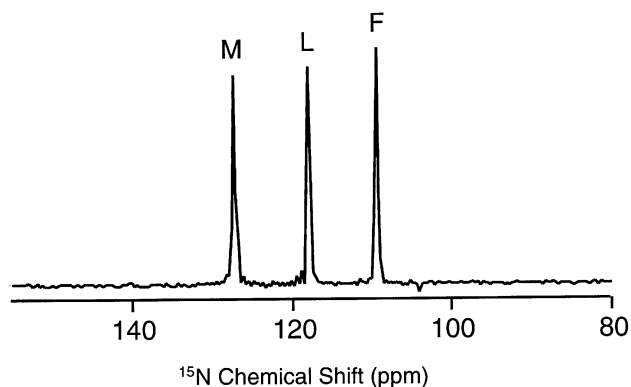


Fig. 4.  $^1\text{H}$  decoupled  $^{15}\text{N}$  CP/MAS spectrum of  $N$ -formyl-[ $^{13}\text{C}$ ,  $^{15}\text{N}$ ]MLF-OH.

$$\Omega_1^{(r)} = \sqrt{\left(n\omega_R \pm \sqrt{\omega_{1S}^2 + (\Omega_S^{(r)})^2}\right)^2 - \omega_{1I}^2} \quad (2)$$

and the dispersion between the two spin pairs ( $r$ ) and ( $s$ ) in the indirect dimension amounts to

$$\delta(r, s) = \Omega_1^{(r)} - \Omega_1^{(s)}. \quad (3)$$

Thus, the frequency dispersion is explicitly dependent upon the choice of the r.f. fields during the SPECIFIC CP transfer and, moreover, on the chemical shifts in the observed ( $S$  spin) dimension. Only if these parameters are of comparable size, can we expect a variation of the frequency dispersion. Since peptide backbone chemical shifts usually span about 20 and 30 ppm in  $^{13}\text{C}$  and  $^{15}\text{N}$ , respectively, a small number of 1D experiments is sufficient to obtain the complete correlation map. This approach can readily be extended to transfer polarization among the side chain ( $^{13}\text{C}$ ) resonances.

### 3. Results and discussion

#### 3.1. Heteronuclear correlation in $N$ -formyl-[ $^{13}\text{C}$ , $^{15}\text{N}$ ]MLF-OH

We employed a uniformly  $^{13}\text{C}$ ,  $^{15}\text{N}$  labeled tripeptide, i.e.,  $N$ -formyl-[ $^{13}\text{C}$ ,  $^{15}\text{N}$ ]MLF-OH to demonstrate the features of the SPECIFIC CP technique that make it useful in a variety of assignment strategies. The spectral assignments of this model tripeptide are described elsewhere [26,36], and we use them for convenience in this contribution. In particular, the  $^{15}\text{N}$  resonances are at 127.3 ppm (Met), 117.9 ppm (Leu), and 109.4 ppm (Phe), as is illustrated in the  $^{15}\text{N}$  CP/MAS spectrum shown in Fig. 4.

The use of SPECIFIC CP to obtain heteronuclear correlations is demonstrated first in Figs. 5a and b where the  $\text{C}_\alpha$  region of the  $^{13}\text{C}$  spectrum of  $N$ -formyl-[ $^{13}\text{C}$ ,  $^{15}\text{N}$ ]MLF-OH is displayed vs. the  $^{15}\text{N}$  offset frequency ( $\Omega_N$ ). In both of these panels, the non-observe ( $^{15}\text{N}$ )

carrier frequency is changed continuously over an interval of 3.6 kHz to cover the  $n = +1$  zero quantum SPECIFIC CP matching condition of all spin pairs ( $\omega_{1S} = 1.8$  kHz,  $\omega_{1I} = 7.2$  kHz, and  $\omega_R = 9.0$  kHz). The difference between the two panels is the carrier frequency of the  $^{13}\text{C}$  observe channel: in 5a the carrier is set downfield from the  $\text{C}_\alpha$  resonances, at 60.6 ppm, while in 5b it is upfield from the  $\text{C}_\alpha$  resonances, at 49.4 ppm (as indicated by asterisk in the figures). In both cases, the positions of the recoupled peaks are completely determined by the r.f. fields, offsets, and MAS frequency ( $\Omega_1$ ,  $\omega_{1I}$ ,  $\Omega_S$ ,  $\omega_{1S}$ , and  $\omega_R$ ) and can be used to resolve ambiguities in larger systems or compounds where the analysis is complicated by linebroadening. The linewidth in the  $^{15}\text{N}$  dimension is determined by the effective dipolar coupling, and is obviously larger than observed in normal HETCOR experiments. However, our measure of resolution in the non-observe dimension of the SPECIFIC HETCOR experiment is the difference in the frequencies of maximal transfer. It is also evident that the resolution in the  $^{15}\text{N}$  dimension differs between the two panels in Figs. 5a and b. In fact, the dispersion between the M and L, and L and F peaks is 0.75 and 0.40 kHz, respectively in Fig. 5a, and 0.20 and 0.65 kHz, respectively in Fig. 5b, while the actual chemical shift differences are 0.47 and 0.43 kHz, respectively. The increased resolution in the SPECIFIC HETCOR experiments may prove very useful for intra-residue assignments in more complicated solid state systems.

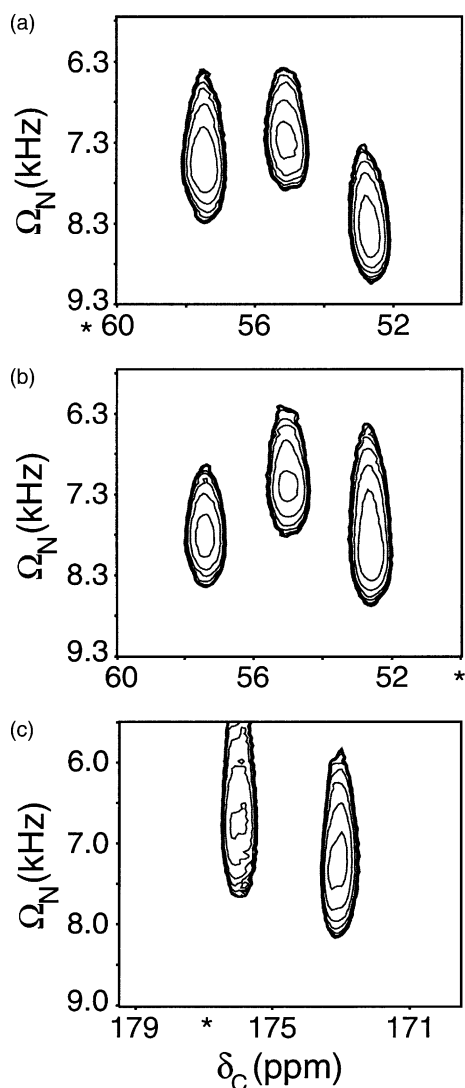
Fig. 5c displays an example of the application of the SPECIFIC CP experiment for inter-residue correlations. The system is again  $N$ -formyl-[ $^{13}\text{C}$ ,  $^{15}\text{N}$ ]MLF-OH, and therefore only two NH-CO pairs are available to participate in the heteronuclear transfer. Simply changing the carrier frequency on the observe channel (to 177 ppm) is sufficient to provide transfer exclusively to the carbonyl region. The r.f. fields and offsets selected for optimal transfer in Fig. 5 give rise to an effective dipolar coupling of  $\sim 67\%$  of the on-resonance  $^{15}\text{N}$ - $^{13}\text{C}$  coupling. Therefore, a 50% longer contact time has to be used compared to an on-resonance transfer (1.5–2.0 ms for a directly bonded N-C pair). Additional relaxation effects result in experimentally determined optimal mixing times of 1.8 ms (for the shorter peptide bond distance, Fig. 5c) and 2.5 ms (for the smaller NH-C $\alpha$  coupling, Figs. 5a and b). All other parameters are essentially the same for NH-CO and NH-C $\alpha$  polarization transfers. In both cases, we observe increased resolution in the indirect dimension compared to the conventional HETCOR experiment.

The efficiency of the  $n = +1$  ZQ SPECIFIC CP in  $N$ -formyl-[ $^{13}\text{C}$ ,  $^{15}\text{N}$ ]MLF-OH is illustrated in Fig. 6. The direct  $^{13}\text{C}$  CP/MAS spectrum is shown in Fig. 6a. As expected, the formyl CO resonance is absent since the group was not  $^{13}\text{C}$  labeled. The spectra displayed in Figs. 6b–e demonstrate the high efficiency of the trans-

fer: 60–62% for the CO's and 55–56% for the three  $C_\alpha$ 's (determined by comparing the S/N of the SPECIFIC CP filtered spectra with the S/N of the direct CP/MAS spectrum in Fig. 6a). It is evident that high efficiency and complete selectivity cannot be achieved simultaneously. In principle, employing adiabatic SPECIFIC CP could increase the efficiency (and decrease the offset dependence) of the transfer. However, relaxation processes may prevent the attainment of the theoretical maximum.

### 3.2. Homonuclear correlation in *N*-formyl-[ $U$ - $^{13}C$ , $^{15}N$ ]MLF-OH

Next, we investigate extensions of the approach discussed so far that enable sequential assignment across the side chain. For this reason we extend the pulse sequence by a homonuclear correlation unit of variable amplitude  $\omega_{1CC}$  and spin lock time  $t_m$  (Fig. 3). As discussed earlier, homonuclear polarization transfer may result if the  $n = 0$  or  $n = 1, 2$  conditions in Eq. (1) are



fulfilled. In Fig. 7, we use scalar and dipolar transfer to map out the  $C_\alpha$ - $C_\beta$  connectivities in *N*-formyl-[ $U$ - $^{13}C$ ,  $^{15}N$ ]MLF-OH. As in Fig. 5, the initial heteronuclear recoupling between all NH- $C_\alpha$  pairs is enabled as the  $^{15}N$  carrier frequency is varied stepwise. Subsequently, homonuclear recoupling transfers polarization through-bond (7a) or through-space (7b) to the  $C_\beta$  region. In Fig. 7a a homonuclear contact time of 5.0 ms and an r.f. field of  $3.0 \pm 0.5$  kHz (ramp from 3.5 to 2.5 kHz) were used. In Fig. 7b, a mixing time of 1.5 ms and an r.f. field strength of  $4.0 \pm 0.5$  kHz were employed. For the latter case, the DQ recoupling condition ( $n = 1$ ) is fulfilled and negative  $C_\beta$  signals (indicated in bold) occur [17,37]. The r.f. fields used for both heteronuclear and homonuclear transfer steps were thus smaller than 10 kHz and 36 1D experiments (0.1 kHz increments of the  $^{15}N$  frequency) were sufficient to generate the results of Fig. 7.

In Fig. 8 we demonstrate that selective transfer can be used to study different spin sub-systems in uniformly labeled compounds. As an example, two sets of side chain correlations are shown using different experimental settings. The MAS frequency was kept constant at 9.0 kHz. In Fig. 8a, the r.f. field during the homonuclear transfer step and the  $^{13}C$  carrier frequency were chosen to be  $4.5 \pm 0.5$  kHz and  $-1.0$  kHz, respectively, with a mixing time of 2.0 ms. As a result, a transfer to the  $\beta$  and  $\gamma$  carbons occurs, as demonstrated by the negative and positive signal intensities, respectively. Such a 'down-up' pattern [17,37,38] indicates that broadband DQ transfer has occurred over two bonds. In

Fig. 5. SPECIFIC HETCOR experiments showing the NH- $C_\alpha$  (a, b) and NH-CO (c) correlations in *N*-formyl-[ $U$ - $^{13}C$ ,  $^{15}N$ ]MLF-OH. In conventional HETCOR [14], the observation of the indirect dimension (the I spins) is realized by  $t_1$  evolution, and the peaks positions in the indirect dimension correspond directly to the chemical shifts of the I spins. In SPECIFIC CP the indirect dimension is obtained by stepping through the frequency range of the (usually  $n = 1$ ) matching conditions of the spins (usually many fewer points are required to construct the 2D correlations) and the peak positions in the indirect dimension correspond to the frequency offsets at which maximal SPECIFIC CP transfer has occurred. The only parameter changed between (a) and (b) is the carrier frequency on the observe channel, identified in the figure by an asterisk. In (a)  $\Omega_C = 0.75$  kHz = 6.0 ppm and in (b)  $\Omega_C = -0.65$  kHz = -5.2 ppm. This change of the  $^{13}C$  offsets, and consequently the effective r.f. fields, leads to different dispersions in the indirect dimension: in (a)  $\delta(M,L) = 0.75$  kHz and  $\delta(L,F) = 0.40$  kHz, while in (b)  $\delta(M,L) = 0.20$  kHz and  $\delta(L,F) = 0.65$  kHz. These frequency differences compare favorably with the absolute chemical shift differences of 0.47 kHz (M,L) and 0.43 kHz (L,F). In both cases,  $\omega_{1C} = 1.8$  kHz,  $\omega_{1N} = 7.2$  kHz,  $\omega_R = 9.0$  kHz, the mixing time  $t_{SP}$  was 2.5 ms, and the spectrometer  $^1H$  frequency was 500 MHz. Contour levels start at 20% of the highest peak in the respective 1D spectra.  $\Omega_N$  was incremented in 72 steps by 0.05 kHz, and 8 transients were collected for each 1D spectrum. In (c) all parameters are identical to those in (a), except that the mixing time  $t_{SP}$  was 1.8 ms and  $\Omega_C = 0.37$  kHz = 3.0 ppm, leading to  $\delta(L,F) = 0.55$  kHz compared to the true chemical shift separation of 0.43 kHz. In Figs. 5–9 the  $^{13}C$  and  $^{15}N$  offsets,  $\Omega_C$  and  $\Omega_N$ , are given relative to the middle resonance of the corresponding (CO,  $C_\alpha$  or NH) triplet.

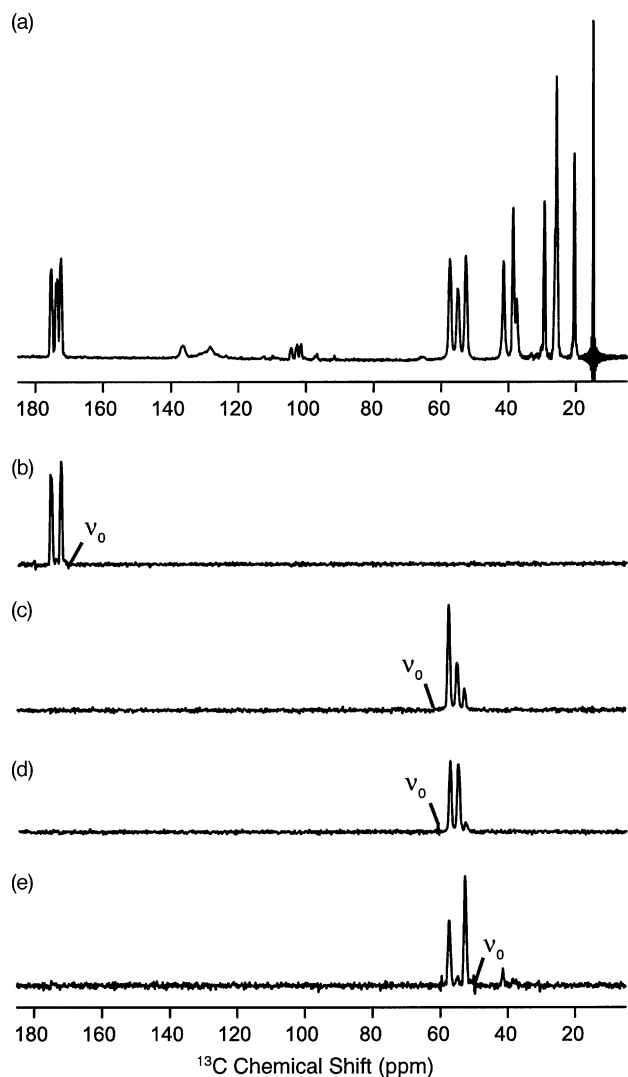


Fig. 6. Demonstration of the SPECIFIC CP transfer efficiency in *N*-formyl-[U- $^{13}\text{C}$ ,  $^{15}\text{N}$ ]MLF-OH. (a) Direct  $^1\text{H}$  to  $^{13}\text{C}$  CP/MAS. (b)–(e) SPECIFIC CP applied at the  $n = +1$  matching condition, with  $\omega_{1\text{C}} = 2.0$  kHz and  $\omega_{1\text{N}} = 7.0$  kHz, and optimized for: (b) the CO resonances to S/N of 60% and 62% of the direct CP/MAS signal with  $\Omega_{\text{C}} = -0.40$  kHz =  $-3.2$  ppm,  $\Omega_{\text{N}} = 7.65$  kHz =  $151.0$  ppm and  $1.8$  ms mixing time; (c) the downfield  $\text{C}_\alpha$  resonance to S/N of 56% with  $\Omega_{\text{C}} = 0.75$  kHz =  $6.0$  ppm,  $\Omega_{\text{N}} = 8.2$  kHz =  $161.8$  ppm and  $2.5$  ms mixing time; (d) the middle  $\text{C}_\alpha$  resonance to S/N of 55% with  $\Omega_{\text{C}} = 0.75$  kHz =  $6.0$  ppm,  $\Omega_{\text{N}} = 7.85$  kHz =  $154.9$  ppm and  $2.5$  ms mixing time; and (e) the upfield  $\text{C}_\alpha$  resonance to S/N of 55% (if 16 transients were taken as for the other four spectra) with  $\Omega_{\text{C}} = -0.65$  kHz =  $-5.2$  ppm,  $\Omega_{\text{N}} = 8.65$  kHz =  $170.7$  ppm and  $2.5$  ms mixing time. The above offsets,  $\Omega_{\text{C}}$  and  $\Omega_{\text{N}}$ , are relative to the middle resonance of the corresponding (CO,  $\text{C}_\alpha$  or NH) triplet. All experiments were performed at  $\omega_{\text{R}} = 9.0$  kHz, ambient temperature and a  $^1\text{H}$  frequency of  $500$  MHz.

Fig. 8b, the experimental conditions were modified to an r.f. field of  $3.5 \pm 0.5$  kHz, a carrier offset of  $+0.75$  kHz, and a mixing time of  $2.5$  ms. The  $\text{C}_\gamma$  intensities of residues M and L are now found to be negative, consistent with long range, two-bond, dipolar (DQ) transfer for  $\text{C}_\alpha$  to  $\text{C}_\gamma$  or DQ transfer from  $\text{C}_\alpha$  to  $\text{C}_\beta$  and a subsequent

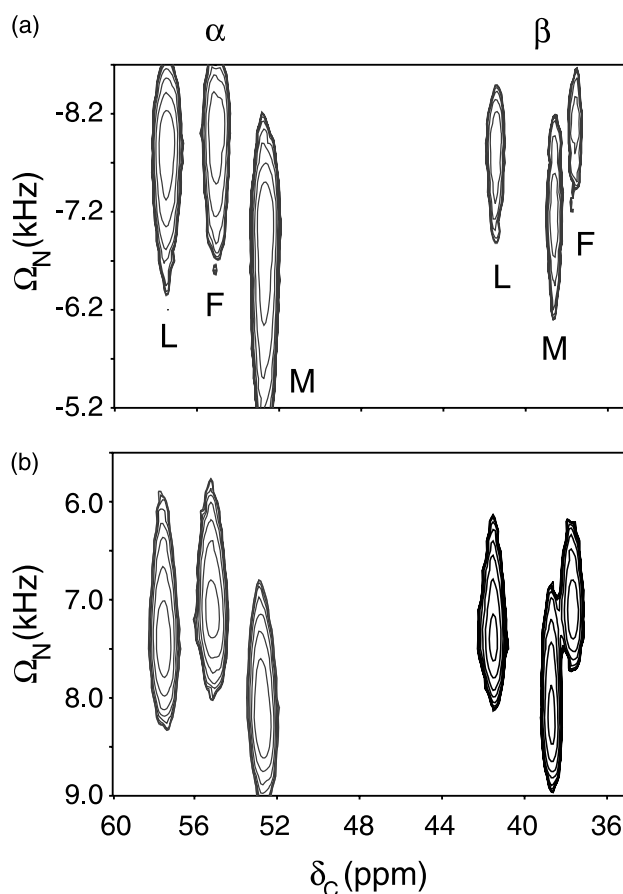


Fig. 7. NH- $\text{C}_\alpha$ - $\text{C}_\beta$  correlations in *N*-formyl-[U- $^{13}\text{C}$ ,  $^{15}\text{N}$ ]MLF-OH using scalar (a) or dipolar (b) couplings. As shown in Fig. 3, an additional r.f. field ( $\omega_{1\text{CC}}$ ) is applied for the homonuclear mixing time  $t_m$ . In (a)  $\Omega_{\text{C}} = -0.84$  kHz,  $t_m = 5.0$  ms, and  $\omega_{1\text{CC}} = 3.0 \pm 0.5$  kHz. 48 transients were acquired for each 1D spectrum. In (b)  $\Omega_{\text{C}} = 0.75$  kHz,  $t_m = 1.5$  ms, and  $\omega_{1\text{CC}} = 4.0 \pm 0.5$  kHz. 64 transients were averaged for each 1D spectrum. The initial NH- $\text{C}_\alpha$  transfer was established by heteronuclear SPECIFIC CP as in Fig. 5.

ZQ (scalar mediated) transfer from  $\text{C}_\beta$  to  $\text{C}_\gamma$ . In any case, both experiments allow for the examination of transfer characteristics in multiply labeled compounds, and can be used in conjunction with numerical simulations to probe the local side chain geometry in fully labeled systems. In the following experiments we focus on heteronuclear backbone correlations.

### 3.3. Heteronuclear correlation in *N*-formyl-[U- $^{15}\text{N}$ ]MLF-OH

The high transfer efficiency of SPECIFIC CP permits applications in  $^{15}\text{N}$  labeled compounds with natural abundance  $^{13}\text{C}$ . These systems have the advantage of improved resolution in the  $^{13}\text{C}$  dimension as the  $^{13}\text{C}$  lines are not broadened by additional large  $J$  couplings. Furthermore, the  $^{15}\text{N}$  compounds are relatively easy and economical to prepare. In Fig. 9 we demonstrate this possibility using *N*-formyl-[U- $^{15}\text{N}$ ]MLF-OH. In an ex-

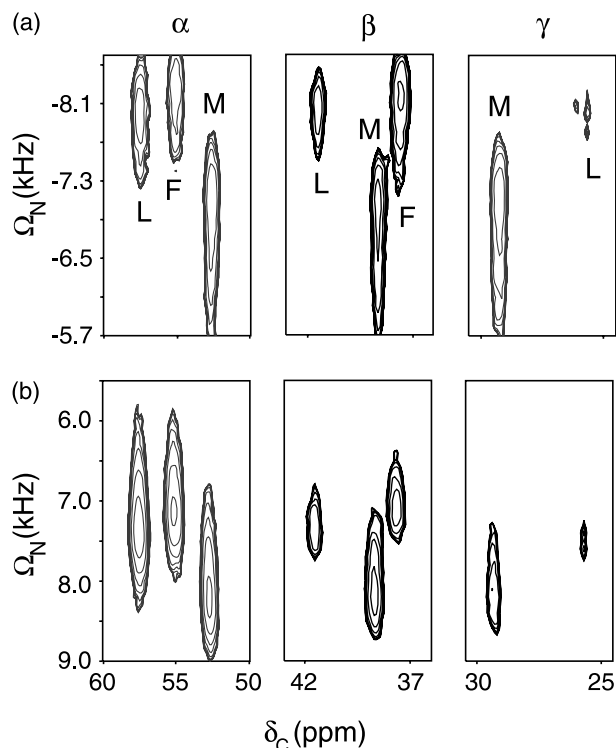


Fig. 8. NH–C $\alpha$ –C $\beta$ –C $\gamma$  correlations in *N*-formyl-[U- $^{13}\text{C}$ ,  $^{15}\text{N}$ ]MLF-OH using dipolar couplings. In (a)  $\omega_{1\text{CC}} = 4.5 \pm 0.5$  kHz,  $t_m = 2.0$  ms, and  $\Omega_{\text{C}} = -1.0$  kHz. In (b)  $\omega_{1\text{CC}} = 3.5 \pm 0.5$  kHz,  $t_m = 3.0$  ms, and  $\Omega_{\text{C}} = 0.75$  kHz were employed. The initial NH–C $\alpha$  transfer was established by heteronuclear SPECIFIC CP as in Fig. 5. The  $^{15}\text{N}$  frequency was incremented by 0.1 kHz in 30 steps (a), and 36 steps (b). 64 transients were acquired for each 1D spectrum.

periment similar to the one shown in Fig. 5, Fig. 9 displays the C $\alpha$  region of the  $^{15}\text{N}$  labeled tripeptide *N*-formyl-MLF-OH. The r.f. fields during the specific CP transfer were initially chosen as 7.0 and 2.0 kHz for  $^{15}\text{N}$  and  $^{13}\text{C}$ , respectively (Fig. 9a). During the experiment, the carrier on the non-observe ( $^{15}\text{N}$ ) channel was stepped over 1.4 kHz within the  $n = +1$  ZQ SPECIFIC CP regime (for the above mentioned r.f. fields and  $\omega_{\text{R}} = 9$  kHz). On the observe ( $^{13}\text{C}$ ) channel, the carrier was placed downfield from the leucine C $\alpha$  peak. Therefore the Phe and Met resonances appear less intense than the Leu (larger  $\Omega_{\text{C}}$  offsets for F and M result in smaller effective dipolar couplings). For comparison, we include slices with numerical predictions for these experimental conditions. In agreement with the experimental findings, we predict a maximum dispersion (i.e. difference in peak positions) of about 0.8 kHz. These experiments were repeated using r.f. fields of about 8 and 1 kHz for  $^{15}\text{N}$  and  $^{13}\text{C}$ , respectively and, following considerations from the previous sections, adjusting the overall frequency interval where  $n = +1$  SPECIFIC CP transfer can be expected (Fig. 9b). In agreement with our numerical predictions, the overall shift of the resonances increases to almost 1 kHz. As shown earlier [7],

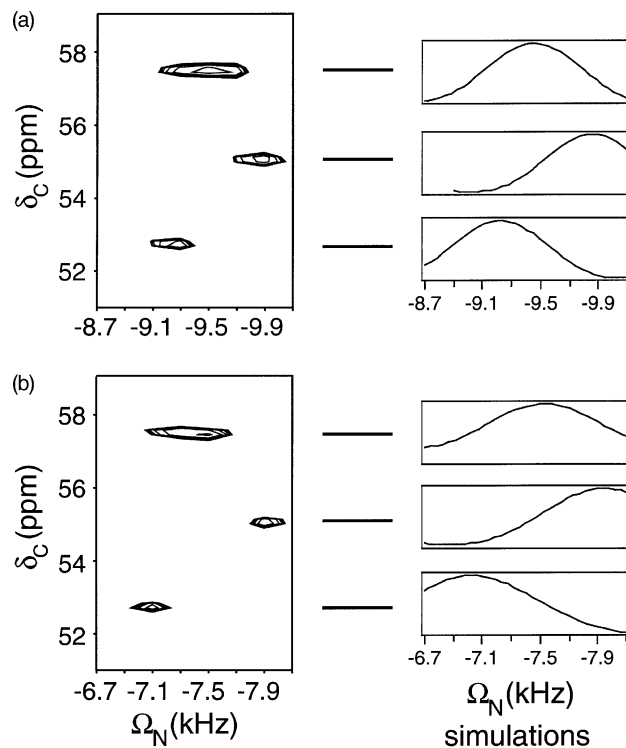


Fig. 9. Experimental application of the SPECIFIC HETCOR experiment to  $^{15}\text{N}$  labeled *N*-formyl- f-MLF-OH displaying NH–C $\alpha$  correlations in the molecule. Changing the r.f. fields for  $^{15}\text{N}$  and  $^{13}\text{C}$  during the SPECIFIC transfer from 7.0 and 2.0 kHz, respectively, in (a) to 8.0 and 1.0 kHz, respectively, in (b) results in modified dispersion and a change in the overall frequency range where transfer occurs. For comparison, numerical simulations (same parameters as in Fig. 1) are shown on the right for each of the three spin pairs.  $\omega_{\text{R}} = 9$  kHz and the  $^1\text{H}$  frequency = 400 MHz. The  $^{15}\text{N}$  frequency was changed in 8 steps, 0.2 kHz each.

the effective dipolar coupling (which represents the bandwidth of the  $n = 1$  SPECIFIC CP excitation in the offset curve) usually increases as the relative r.f. field,  $\omega_{1\text{S}}/\omega_{1\text{H}}$ , is decreased. Thus, the increased dispersion of SPECIFIC recoupling among different spin pairs is usually accompanied by a larger linewidth affecting the overall resolution.

We have already discussed [7] the influence of CSA interactions and resonance offsets on SPECIFIC CP transfer among different spin pairs in a multi-spin system. Examples could include polypeptides with a large number of backbone pairs in which the effective dipolar coupling might change considerably. In these cases, the SPECIFIC HETCOR experiment can yield connectivities with better resolution. In addition, the experimental procedure outlined above can be advantageous whenever subsections of the total spectrum need to be studied and a complete  $t_1$  evolution (with a sufficient number of  $t_1$  increments) is undesirable. Instead, several SPECIFIC HETCOR experiments with varying parameters could be performed to resolve ambiguities in the conventional HETCOR assignment. Again, this method would be of



particular importance in applications with severe spectral overlap. The principles outlined above are also valid for C–N transfer by appropriate adjustment of the r.f. fields involved in the SPECIFIC CP step.

### 3.4. The Ala81–Arg82 peptide bond in bR

The efficiency of the SPECIFIC transfer step also makes applications possible in which signal-to-noise is marginal. As an example, we have applied SPECIFIC CP transfer steps to study single peptide bonds among the 247 peptide bonds in bacteriorhodopsin. Since only one of the seven arginine residues is directly bonded to an alanine,  $^{13}\text{C}$  labeling of the carbonyls of all 29 alanine residues and  $^{15}\text{N}$  labeling of the amino groups of all seven arginine residues, introduces a unique  $^{13}\text{C}$ – $^{15}\text{N}$  pair in the Ala81–Arg82 peptide bond. Fig. 10 compares the results of the SPECIFIC CP experiment with that of the non-selective CP/MAS experiment for light-adapted bR. The top spectra show the signals of 29 alanine carbonyl carbons (left) and seven arginine peptide nitrogens (right), while the bottom spectra show only the signals of  $[1-^{13}\text{C}]\text{Ala81}$  and  $[\alpha-^{15}\text{N}]\text{Arg82}$ . The latter spectra clearly show disorder in the Ala81–Arg82 peptide bond in that the signals from Ala81 and Arg82 span a substantial part of the total linewidth of the 29 alanines and 7 arginines, respectively. This disorder reflects the presence of a number of species with different chemical shifts. Previous REDOR experiments are in agreement with these findings [39].

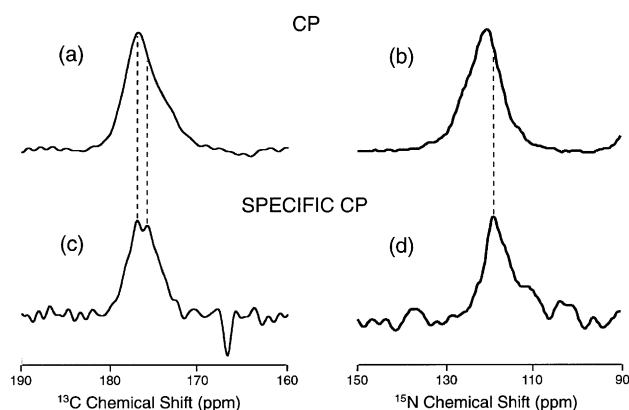


Fig. 10. Direct CP/MAS (top) vs. SPECIFIC CP filtered (bottom)  $^{13}\text{C}$  (left) and  $^{15}\text{N}$  (right) spectra of light-adapted  $[1-^{13}\text{C}]\text{Ala}$ ,  $[\text{U}-^{15}\text{N}]\text{Arg}$ ,  $[\zeta-^{15}\text{N}]\text{Lys}$ -bR. A mixing time of 1.65 ms was used for the C  $\rightarrow$  N transfer with  $\omega_{1\text{N}} = 20.3$  kHz,  $\omega_{1\text{C}} = 22.3$  kHz and  $\Omega_{\text{C}} = 15$  kHz. For the N  $\rightarrow$  C experiment, a mixing time of 1.5 ms was used with  $\omega_{1\text{C}} = 17.1$  kHz,  $\omega_{1\text{N}} = 20.8$  kHz and  $\Omega_{\text{N}} = 10$  kHz. The frequency offsets in the legends for Figs. 10–12,  $\Omega_{\text{C}}$  and  $\Omega_{\text{N}}$ , are given with respect to the highest peak in the broad resonance of the corresponding direct CP/MAS spectrum.  $\omega_{\text{R}} = 4.3$  kHz was used and all data were collected at  $-90^\circ\text{C}$  at 317 MHz  $^1\text{H}$  frequency. Fig. 10b also shows part of the  $^{15}\text{N}$  arginine side chain resonances (87–73 ppm), and the sharp negative peak at 166.2 ppm in Fig. 10c is due to the carrier frequency. On average,  $1.8 \times 10^4$  transients were acquired per spectrum.

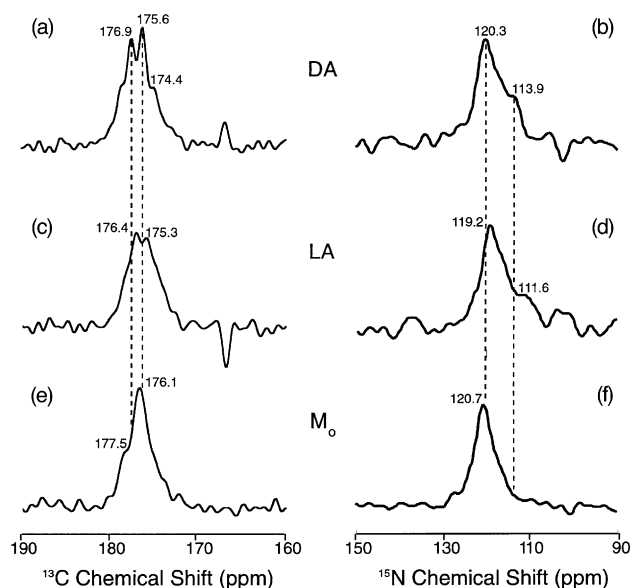


Fig. 11. SPECIFIC CP filtered  $^{13}\text{C}$  (left) and  $^{15}\text{N}$  (right) spectra of  $[1-^{13}\text{C}]\text{Ala}$ ,  $[\text{U}-^{15}\text{N}]\text{Arg}$ ,  $[\zeta-^{15}\text{N}]\text{Lys}$ -bR for different cryo-trapped photocycle intermediates. All conditions are as in Fig. 10. The feature at  $\sim 166$  ppm in spectra (a) and (c), and at  $\sim 100$  ppm in spectra (b) and (d), is due to the carrier frequency.

Fig. 11 shows SPECIFIC CP spectra for three different states of the protein-dark adapted (DA), light adapted (LA), and an early  $M_0$  state. The disorder in the Ala81–Arg82 peptide bond clearly varies among states in the protein, although chemical shift changes are small. The disorder is not much less in the DA state than in the LA state, even though it comprises a mixture of LA and a second species. The disorder is smallest in the  $M_0$  state, even though it is an intermediate in the photocycle of LA. This is the first time we have observed substantial disorder that varies among the bR photocycle intermediates.

### 3.5. The Val49–Pro50, Val69–Pro70, and Val199–Pro200 peptide bonds in bR

Examination of the bR amino acid sequence shows that three of the eleven proline residues follow valine residues. As with the Ala81–Arg82 pair, our idea is to isolate the carbonyl resonances arising from the V49–P50, V69–P70, and V199–P200 pairs by using the dipolar filtering features of the SPECIFIC CP technique on  $[\alpha-^{15}\text{N}]\text{Pro}$ ,  $[1-^{13}\text{C}]\text{Val}$ -bR. We step through the  $^{15}\text{N}$  frequency to obtain the offsets at which the maximum transfer (NH  $\rightarrow$  CO) occurs for the three pairs, and utilize this information to correlate the  $^{13}\text{C}$  and  $^{15}\text{N}$  resonances.

The SPECIFIC HETCOR spectra obtained in this manner are presented in Fig. 12a. The projection of the 2D  $^{13}\text{C}$ ,  $^{15}\text{N}$  spectrum from Fig. 12a is shown in Fig. 12b. As can be seen from both Figs. 12a and b, the three carbonyl resonances give rise to only two lines, at 173.2 and

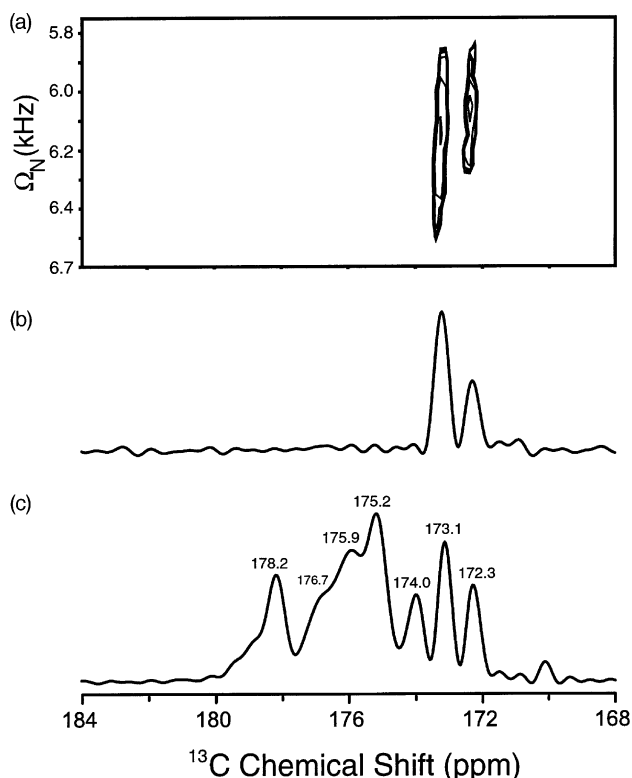


Fig. 12.  $^{13}\text{C}$  SPECIFIC HETCOR in the DA state of  $[\alpha\text{-}^{15}\text{N}]\text{Pro}, [1\text{-}^{13}\text{C}]\text{Val-bR}$  at  $1^\circ\text{C}$ . (a)  $^{15}\text{N}$  to  $^{13}\text{C}$  SPECIFIC CP transfer with  $\omega_{1\text{C}} = 1.4\text{ kHz}$ ,  $\omega_{1\text{N}} = 5.5\text{ kHz}$ ,  $\Omega_{\text{C}} = -0.2\text{ kHz}$ , and  $1.8\text{ ms}$  mixing time. 3200 transients were accumulated for each of the 18  $^{15}\text{N}$  frequencies,  $\Omega_{\text{N}} = [6.70, 6.60, 6.50, 6.45, 6.40, \dots, 5.90, 5.85, 5.80, 5.70]\text{ kHz}$ . The  $^{13}\text{C}$  carbonyl nuclei are recoupled at different  $^{15}\text{N}$  frequency offsets, thereby allowing the assignment of the resonances. In this case (as for *N*-formyl-MLF-OH) the  $^{13}\text{C}$  and  $^{15}\text{N}$  offsets,  $\Omega_{\text{C}}$  and  $\Omega_{\text{N}}$ , are given relative to the middle resonance of the corresponding triplet. Contour levels start at 57% of the maximum transfer peak for the respective resonance. (b) represents a combination of the data from (a). Two of the carbonyls contribute to the intensity of the  $173.2\text{ ppm}$  line, while the third carbonyl resonance is at  $172.3\text{ ppm}$ . (c)  $^{13}\text{C}$  direct detection CP/MAS spectrum of the 21 valine residues in bR obtained by averaging of 3840 transients.  $\omega_{\text{R}} = 6.9\text{ kHz}$  and the  $317\text{ MHz}$  ( $^1\text{H}$  frequency) spectrometer were used. The data were collected at  $1^\circ\text{C}$  to take advantage of the increased spectral resolution observed at temperatures above freezing.

$172.3\text{ ppm}$ , in a 2:1 intensity ratio. For purposes of comparison, the direct ( $^1\text{H} \rightarrow ^{13}\text{C}$ ) CP/MAS spectrum of all 21 valine residues in bR is shown in Fig. 12c. All of these spectra at  $1^\circ\text{C}$  exhibit relatively good resolution (FWHM  $< 0.5\text{ ppm}$ ). The  $^{15}\text{N}$  direct CP/MAS spectrum of the 11 prolines at  $1^\circ\text{C}$  (results not shown) is in full agreement with the room temperature spectra obtained previously (Farrar, M. R. 1991, unpublished results, [28]). In addition,  $^{15}\text{N}$  REDOR experiments on the DA state of  $[\alpha\text{-}^{15}\text{N}]\text{Pro}, [1\text{-}^{13}\text{C}]\text{Val-bR}$  at room temperature, identify the chemical shifts of the imide nitrogens of the three prolines as  $132.7$ ,  $135.7$ , and  $143.7\text{ ppm}$  [28]. We now proceed with the  $^{13}\text{C}$ ,  $^{15}\text{N}$  correlations. Since the SPECIFIC HETCOR spectrum in Fig. 12a clearly shows

significant polarization transfer at relatively high  $^{15}\text{N}$  offsets, one of the Val-Pro pairs has  $^{13}\text{C}$  and  $^{15}\text{N}$  chemical shifts of  $173.2$  and  $143.7\text{ ppm}$ , respectively. Due to the coincidence of two of the  $^{13}\text{C}$  peaks and the small separation between the two nitrogen resonances (less than  $100\text{ Hz}$ ), we need to consider the two possibilities for the remaining  $^{13}\text{C}$ ,  $^{15}\text{N}$  correlations, i.e. (a) ( $173.2$ ,  $135.7\text{ ppm}$ ) and ( $172.3$ ,  $132.7\text{ ppm}$ ) versus (b) ( $173.2$ ,  $132.7\text{ ppm}$ ) and ( $172.3$ ,  $135.7\text{ ppm}$ ). The SPECIFIC CP transfer curves for the  $^{13}\text{C}$  peaks at  $173.2$  and  $172.3\text{ ppm}$  show maxima at  $^{15}\text{N}$  offsets of  $6.15\text{ kHz}$  and  $6.05\text{ kHz}$ , respectively. The  $6.15\text{ kHz}$  maximum falls approximately in the middle between the maxima of the two corresponding nearly symmetric transfer curves. If we now calculate (using Eq. (2)) the frequency difference between the offsets at which maximum transfers would occur, we obtain  $0.24\text{ kHz}$  (case a) and  $0.10\text{ kHz}$  (case b) compared to  $0.10\text{ kHz}$  (actual data). Since the experimental  $^{15}\text{N}$  resolution (steps of  $0.05\text{ kHz}$ ) and  $^{13}\text{C}$  S/N are sufficiently high, we conclude that the signals are correlated as in case b. Therefore the  $^{13}\text{C}$  carbonyl and  $^{15}\text{N}$  amide chemical shifts of the Val49-Pro50, Val69-Pro70, and Val199-Pro200 pairs are: ( $173.2$ ,  $132.7$ ), ( $172.3$ ,  $135.7$ ), and ( $173.2$ ,  $143.7\text{ ppm}$ ). These data on  $[\alpha\text{-}^{15}\text{N}]\text{Pro}, [1\text{-}^{13}\text{C}]\text{Val-bR}$  show that heteronuclear correlation information is easily achievable with few 1D SPECIFIC CP experiments, even in large membrane proteins. In multiply labeled systems, this approach and additional homonuclear recoupling experiments could greatly facilitate the assignment of the backbone resonances.

#### 4. Conclusions

As in liquid-state NMR, backbone and side chain resonance assignment methods form the basis for studies of structure and dynamics in multiply labeled solid-phase polypeptides and proteins. We have demonstrated a correlation experiment (SPECIFIC HETCOR) that enables these studies with no restriction on  $^{13}\text{C}$  or  $^{15}\text{N}$  labeling, and with high efficiency. Because the SPECIFIC CP transfer is explicitly dependent on the resonance offsets, backbone assignments have been accomplished in a model peptide with a small number of 1D experiments. In the version described here, the carrier frequency on the non-observe low- $\gamma$  channel is stepped through the offset region of interest, thereby reducing the total acquisition time relative to a conventional 2D HETCOR. As demonstrated for f-MLF-OH, the experiment can easily be extended to investigate side chain connectivities. Since the SPECIFIC HETCOR pattern depends on the choice of r.f. fields and offsets, ambiguities in larger systems can be resolved with spectra obtained under different experimental conditions, together with a simple algebraic analysis. Alternatively, the SPECIFIC CP transfer mechanism

can be employed during the mixing time of a regular 2D  $^{15}\text{N}$ - $^{13}\text{C}$  HETCOR experiment. Applications in uniformly  $^{13}\text{C}$ ,  $^{15}\text{N}$  labeled peptides and membrane proteins have been demonstrated recently [40–43].

Our results indicate that the efficiency of the transfer also allows applications in  $^{15}\text{N}$  labeled polypeptides with natural abundance  $^{13}\text{C}$  and in  $^{13}\text{C}$ ,  $^{15}\text{N}$  labeled membrane proteins.  $^{15}\text{N}$  labeled peptides with natural abundance  $^{13}\text{C}$  are not only easier to obtain than  $^{13}\text{C}$  and  $^{15}\text{N}$  labeled samples, but the undesirable linebroadening due to homonuclear  $^{13}\text{C}$  scalar couplings is also circumvented. As an application to a much larger protein, we have studied the Ala81–Arg82 peptide bond in  $[1\text{-}^{13}\text{C}]\text{Ala}$ ,  $[\text{U-}^{15}\text{N}]\text{Arg}$ ,  $[\zeta\text{-}^{15}\text{N}]\text{Lys}$  labeled bacteriorhodopsin in different photocycle intermediates. It has been shown that Arg82 is a crucial part of the proton transfer pathway on the extracellular side of the protein. In our study, we find that photocycle intermediates differ in the overall line-shape and linewidth of the Arg82 amide and Ala81 carbonyl resonances, which is indicative of “dynamical” disorder during the photocycle. Further information might be gained by combining the present approach with the homonuclear transfer technique discussed in this manuscript. The potential of the technique to elucidate backbone topologies in NH–CO regions has been demonstrated in  $[\alpha\text{-}^{15}\text{N}]\text{Pro}$ ,  $[1\text{-}^{13}\text{C}]\text{Val}$  labeled bR. To our knowledge, this experiment is the first to investigate backbone correlations in a membrane protein without time-consuming multi-dimensional experiments.

The SPECIFIC CP technique is very forgiving with respect to hardware requirements, and can easily be combined with homonuclear transfer techniques. Efficient polarization transfer into the side chain region of multiply labeled peptides has been demonstrated using r.f. CW fields on the order of 1–10 kHz. We expect the technique to be useful for large, multiply-labeled immobilized peptides and proteins, in which S/N issues are crucial. In systems where proton interactions can be reduced by rapid sample spinning or deuterium dilution, the present methods can be applied in standard HRMAS assemblies.

## Acknowledgments

We thank Drs. Chad M. Rienstra, Jingui G. Hu, and John D. Gross for the design and construction of the transmission line probes employed in these experiments, and Dr. Hong Ni for providing the transparent K-treated pyrex rotors used for the cryo-trapping of the bR photocycle intermediates. Dr. Marc Baldus acknowledges financial assistance from the Deutsche Forschungsgemeinschaft. The research was supported by the National Institutes of Health (GM-36810, GM-23289, and RR-00995).

## References

- [1] M. Ikura, L.E. Kay, A. Bax, A novel approach for sequential assignment of  $^1\text{H}$ ,  $^{13}\text{C}$ , and  $^{15}\text{N}$  spectra of larger proteins: heteronuclear triple-resonance three-dimensional NMR spectroscopy. Application to calmodulin, *Biochemistry* 29 (1990) 4659–4667.
- [2] E.R. Andrew, A. Bradbury, R.G. Eades, Nuclear magnetic resonance spectra from a crystal rotated at high speed, *Nature* 182 (1958) 1659.
- [3] I.J. Lowe, Free induction decays of rotating solids, *Phys. Rev. Lett.* 2 (1959) 285.
- [4] S.J. Opella, J.S. Waugh, Two-dimensional  $^{13}\text{C}$  NMR of highly oriented polyethylene, *J. Chem. Phys.* 66 (1977) 4919–4924.
- [5] C.R. Sanders, B.J. Hare, K.P. Howard, J.H. Prestegard, Magnetically-oriented phospholipid micelles as a tool for the study of membrane-associated molecules, *Progr. NMR Spectrosc.* 26 (1994) 421–444.
- [6] R.S. Prosser, J.S. Hwang, R.R. Vold, Magnetically aligned phospholipid bilayers with positive ordering: a new model membrane system, *Biophys. J.* 74 (1998) 2405–2418.
- [7] M. Baldus, A.T. Petkova, J. Herzfeld, R.G. Griffin, Cross polarization in the tilted frame: assignment and spectral simplification in heteronuclear spin systems, *Molec. Phys.* 95 (1998) 1197–1207.
- [8] S.R. Hartmann, E.L. Hahn, Nuclear double resonance in the rotating frame, *Phys. Rev.* 128 (1962) 2042–2053.
- [9] A. Pines, M.G. Gibby, J.S. Waugh, Proton-enhanced NMR of dilute spins in solids, *J. Chem. Phys.* 59 (1973) 569–590.
- [10] X.L. Wu, K.W. Zilm, Cross polarization with high speed magic angle spinning, *J. Magn. Reson. A* 104 (1993) 154–165.
- [11] G. Metz, X.L. Wu, S.O. Smith, Ramped-amplitude cross-polarization in magic angle spinning NMR, *J. Magn. Reson. A* 110 (1994) 219–227.
- [12] S. Hediger, B.H. Meier, R.R. Ernst, Cross-polarization under fast magic-angle sample-spinning using amplitude-modulated spinlock, *Chem. Phys. Lett.* 213 (1993) 627–635.
- [13] M. Baldus, D.G. Geurts, S. Hediger, B.H. Meier, Efficient  $^{15}\text{N}$ - $^{13}\text{C}$  polarization transfer by adiabatic-passage Hartmann-Hahn cross polarization, *J. Magn. Reson. A* 118 (1996) 140–144.
- [14] A.A. Maudsley, R.R. Ernst, Indirect detection of magnetic resonance by heteronuclear two-dimensional spectroscopy, *Chem. Phys. Lett.* 50 (1977) 368–372.
- [15] S.C. Shekar, A. Ramamoorthy, The unitary evolution operator for cross-polarization schemes in NMR, *Chem. Phys. Lett.* 342 (2001) 127–134.
- [16] N.C. Nielsen, H. Bildsoe, H.J. Jakobsen, M.H. Levitt, Double-quantum homonuclear rotary resonance-efficient dipolar recovery in magic-angle-spinning nuclear-magnetic-resonance, *J. Chem. Phys.* 101 (1994) 1805–1812.
- [17] M. Baldus, M. Tomaselli, B.H. Meier, R.E. Ernst, Broadband polarization transfer experiments for rotating solids, *Chem. Phys. Lett.* 230 (1994) 329–336.
- [18] R. Henderson, J.M. Baldwin, T.A. Ceska, F. Zemlin, E. Beckmann, K.H. Downing, Model for the structure of bacteriorhodopsin based on high-resolution electron cryomicroscopy, *J. Mol. Biol.* 213 (1990) 899–929.
- [19] N. Grigorieff, T.A. Ceska, K.H. Downing, J.M. Baldwin, R. Henderson, Electron-crystallographic refinement of the structure of bacteriorhodopsin, *J. Mol. Biol.* 259 (1996) 393–421.
- [20] L.J. Stern, H.G. Khorana, Structure-function studies on bacteriorhodopsin. X. Individual substitutions of arginine residues by glutamate affect chromophore formation, photocycle, and proton translocation, *J. Biol. Chem.* 264 (1989) 14202–14208.
- [21] G.C. Lin, M.A. El-Sayed, T. Marti, L.J. Stern, T. Mogi, H.G. Khorana, Effects of individual genetic substitutions of arginine

- residues on the deprotonation and reprotonation kinetics of the Schiff base during the bacteriorhodopsin photocycle, *Biophys. J.* 60 (1991) 172–178.
- [22] S.P. Balashov, R. Govindjee, M. Kono, E. Imasheva, E. Lukashiev, T.G. Ebrey, R.K. Crouch, D.R. Menick, Y. Feng, Effect of the arginine-82 to alanine mutation in bacteriorhodopsin on dark adaptation, proton release, and the photochemical cycle, *Biochemistry* 32 (1993) 10331–10343.
- [23] S.P. Balashov, E.S. Imasheva, R. Govindjee, T.G. Ebrey, Titration of aspartate-85 in bacteriorhodopsin: what it says about chromophore isomerization and proton release, *Biophys. J.* 70 (1996) 473–481.
- [24] R. Govindjee, S. Misra, S.P. Balashov, T.G. Ebrey, R.K. Crouch, D.R. Menick, Arginine-82 regulates the  $pK_a$  of the group responsible for the light-driven proton release in bacteriorhodopsin, *Biophys. J.* 71 (1996) 1011–1023.
- [25] A.T. Petkova, J.G. Hu, M. Bizounok, M. Simpson, R.G. Griffin, J. Herzfeld, Arginine activity in the proton-motive photocycle of bacteriorhodopsin: solid-state NMR studies of the wild-type and D85N proteins, *Biochemistry* 38 (1999) 1562–1572.
- [26] M. Hong, R.G. Griffin, Resonance assignments for solid peptides by dipolar-mediated  $^{13}C/^{15}N$  correlation solid-state NMR, *J. Am. Chem. Soc.* 120 (1998) 7113–7114.
- [27] M.B. Gochbauer, D.J. Kushner, Growth and nutrition of extremely halophilic bacteria, *Can. J. Microbiol.* 15 (1969) 1157–1165.
- [28] J.G. Hu, Solid-state NMR studies of bacteriorhodopsin and model compounds: insight into the spectral tuning and the photocycle, Ph.D. Thesis, Brandeis University, 1995.
- [29] J.G. Hu, B.Q. Sun, M. Bizounok, M.E. Hatcher, J.C. Lansing, J. Raap, P.J.E. Verdegem, J. Lugtenburg, R.G. Griffin, J. Herzfeld, Early and late M photointermediates in the bacteriorhodopsin photocycle: a solid state NMR study, *Biochemistry* 37 (1998) 8088–8096.
- [30] D. Oesterhelt, W. Stoekenius, Isolation of the cell membrane of *Halobacterium halobium* and its fractionation into red and purple membrane, *Methods Enzymol.* 31 (1974) 667–678.
- [31] C.M. Rienstra, Multi-channel transmission line probes for high field magic-angle spinning NMR, Ph.D. Thesis, MIT, 1999.
- [32] A.E. Bennett, C.M. Rienstra, M. Auger, K.V. Lakshmi, R.G. Griffin, Heteronuclear decoupling in rotating solids, *J. Chem. Phys.* 103 (1995) 1–8.
- [33] W.L. Earl, D.L. VanderHart, Measurement of  $^{13}C$  chemical shifts in solids, *J. Magn. Reson.* 48 (1982) 35–54.
- [34] J.L. Markley, A. Bax, Y. Arata, C.W. Hilbers, R. Kaptein, B.D. Sykes, P.E. Wright, K. Wüthrich, Recommendations for the presentation of NMR structures of proteins and nucleic acids, *Pure Appl. Chem.* 70 (1998) 117–142.
- [35] D.S. Wishart, C.G. Bigam, J. Yao, F. Abildgaard, H.J. Dyson, E. Oldfield, J.L. Markley, B.D. Sykes,  $^1H$ ,  $^{13}C$  and  $^{15}N$  chemical shift referencing in biomolecular NMR, *J. Biomol. NMR* 6 (1995) 135–140.
- [36] C.M. Rienstra, M. Hohwy, M. Hong, R.G. Griffin, 2D and 3D  $^{15}N$ - $^{13}C$ - $^{13}C$  NMR chemical shift correlation spectroscopy of solids: assignment of MAS spectra of peptides, *J. Am. Chem. Soc.* 122 (2000) 10979–10990.
- [37] B.Q. Sun, P.R. Costa, D. Kocisko, P.T. Lansbury Jr., R.G. Griffin, Internuclear distance measurements in solid state NMR: dipolar recoupling via rotor synchronized spin-locking, *J. Chem. Phys.* 102 (1994) 702–707.
- [38] B.Q. Sun, C.M. Rienstra, P.R. Costa, J.R. Williamson, R.G. Griffin, 3D  $^{15}N$ - $^{13}C$ - $^{13}C$  chemical shift correlation spectroscopy in rotating solids, *J. Am. Chem. Soc.* 119 (1997) 8540–8546.
- [39] A.T. Petkova, B.Q. Sun, M. Bizounok, J.G. Hu, R.G. Griffin, J. Herzfeld, Solid-state NMR studies of the arginine residues in the proton-motive photocycle of bacteriorhodopsin, *Biophys. J.* 72 (1997) A208.
- [40] J. Pauli, M. Baldus, B. van Rossum, H. de Groot, H. Oschkinat, Backbone and side-chain  $^{13}C$  and  $^{15}N$  signal assignments of the  $\alpha$ -spectrin SH3 domain by magic angle spinning solid-state NMR at 17.6 tesla, *Chem. Biochem.* 2 (2001) 272–281.
- [41] T.A. Egorova-Zachernyuk, J. Hollander, N. Fraser, P. Gast, A.J. Hoff, R. Cogdell, H.J.M. de Groot, M. Baldus, Heteronuclear 2D-correlations in a uniformly [ $^{13}C$ ,  $^{15}N$ ] labeled membrane-protein complex at ultra-high magnetic fields, *J. Biomol. NMR* 19 (2001) 243–253.
- [42] A.T. Petkova, Y. Ishii, J.J. Balbach, O.N. Antzutkin, R.D. Leapman, R. Tycko, An experimentally-based structural model for Alzheimer's  $\beta$ -amyloid fibrils, *Proc. Natl. Acad. Sci. USA* 99 (2002) 16742–16747.
- [43] C.M. Rienstra, L. Tucker-Kellogg, C.P. Jaroniec, M. Hohwy, B. Reif, M.T. McMahon, B. Tidor, T. Lozano-Perez, R.G. Griffin, De novo determination of peptide structure with solid-state magic-angle spinning NMR spectroscopy, *Proc. Natl. Acad. Sci. USA* 99 (2002) 10250–10255.
- [44] S.O. Smith, T.O. Levante, B.H. Meier, R.R. Ernst, Computer simulations in magnetic resonance. An object-oriented programming approach, *J. Magn. Reson. A* 106 (1994) 75–105.